CrystEngComm

PAPER

p-CdTe nanoribbon/n-silicon nanowires array heterojunctions: photovoltaic devices and zero-power photodetectors†

Chao Xie,[ab] **Lin-Bao Luo,**[*a] **Long-Hui Zeng,**[a] **Long Zhu,**[a] **Jing-Jing Chen,**[a] **Biao Nie,**[a] **Ji-Gang Hu,**[a] **Qiang Li,**[a] **Chun-Yan Wu,**[a] **Li Wang**[a] **and Jian-Sheng Jie**[*c]

Nano-heterojunction composed of single Sb-doped p-type CdTe nanoribbon (CdTeNR) and n-type silicon nanowires (SiNWs) array was successfully fabricated. The p–n heterojunction exhibited excellent rectifying behavior with a rectification ratio of 10^5 at ± 2 V in the dark. Due to the matched band gap of CdTeNR with SiNWs, as well as the efficient light absorption of the SiNWs array, pronounced photovoltaic characteristics with energy conversion efficiency up to 2.1% under AM 1.5 G was achieved. Furthermore, the heterojunction device could serve as high-performance zero-power photodetector operated in the visible to near-infrared (NIR) range with good stability, high sensitivity, and fast response speed. It is expected that the p-CdTeNR/n-SiNWs array heterojunctions will find important applications in future nano-optoelectronic devices.

Introduction

As an important II–VI semiconductor, CdTe has demonstrated great potential in the applications of optoelectronic devices.[1,2] Owing to the appropriate direct band gap (1.5 eV at room temperature), CdTe is particularly good at absorbing solar light in the visible to ultraviolet (UV) range.[3] This property renders CdTe the most promising material for photovoltaic applications. For instance, Britt *et al.* successfully demonstrated the fabrication of 1 cm² large thin-film CdS/CdTe solar cells with an impressive efficiency of 15.8% under AM 1.5 G illumination.[4] Moreover, by combining several materials with distinct properties, Wu *et al.* reported on a CTO/ZTO/CdS/CdTe polycrystalline thin-film solar cell with efficiency up to 16.5%,[5] the highest values among CdS/CdTe thin-film based solar cells. In addition to photovoltaic devices, CdTe has also found wide application in photodetection.[6,7] Taking single-crystalline CdTe NWs for example, it has been reported that straight CdTe NWs can work as efficient photodetector with high photocurrent decay ratio, high responsivity, and no decay tail.[8] Moreover, CdTe nanoribbons (CdTeNRs) converted from ZnTe NRs exhibited significant photoresponse to visible-NIR illumination with high responsivity and gain.[9]

Another equally important material for photovoltaic application is silicon nanostructure. One dimensional (1D) silicon nanowire (SiNW) arrays, be it synthesized by vapor–liquid–solid (VLS) or metal-assisted chemical etching methods,[10,11] have showed great potential for photovoltaic devices, due to their unique properties in terms of light absorption in the region of visible and near-infrared light[12] and electron transport.[13] For example, by depositing a p-type amorphous Si thin-film on the surface of etched SiNWs, Garnett *et al.* demonstrated the construction of core-shell p–n junction solar cells with efficiency of nearly 0.5%.[14] Furthermore, by using multicrystalline p^+nn^+-doped silicon layers, Sivakov *et al.* successfully fabricated SiNWs array solar cells on glass substrates with maximum efficiency of 4.4%.[15] Such SiNWs array based devices exhibit low reflectance (<10%, at 300–800 nm) and strong broadband optical absorption (>90% at 500 nm).

In spite of these progresses, the above homojunction-based photovoltaic devices usually suffer from either weak absorption of short-wave solar light, or electrical losses which greatly reduce the energy conversion efficiency. In light of this, nano-heterojunctions consisting two or more materials with different band gaps are introduced into the device. It is found that due to different wavelength coverage, such novel structures could enable more effective light absorption, and thus greatly increase the energy conversion efficiency.[16,17] In this paper, we present the fabrication of a nano-heterojunction composed of single Sb-doped p-CdTeNR and n-SiNWs array. Electrical measurement reveals that the as-prepared p–n junction showed well-defined rectifying effect with rectification ratio of 10^5 at ± 2 V at room temperature. The energy band diagram of the heterojunction under light illumination was plotted to illustrate the working mechanism of the photovoltaic behavior of the p-CdTeNR/n-SiNWs array

aSchool of Electronic Science and Applied Physics, Hefei University of Technology, Hefei, Anhui, 230009, P. R. China. E-mail: luolb@hfut.edu.cn
bSchool of Materials Science and Engineering, Hefei University of Technology, Hefei, Anhui, 230009, P. R. China
cInstitute of Functional Nano & Soft Materials (FUNSOM) and Jiangsu Key Laboratory for Carbon-Based Functional Materials & Devices, Soochow University, Suzhou, Jiangsu, 215123, P. R. China. E-mail: jsjie@suda.edu.cn
† Electronic supplementary information (ESI) available. See DOI: 10.1039/c2ce25791b

heterojunction devices. Furthermore, without applying bias voltage, such heterojunction devices can work as photodetectors for visible-NIR illumination with good stability, high photosensitivity as well as fast response speed in a wide range of switching frequencies.

Experimental section

Materials synthesis and characterization

In this study, the fabrication of the nano-heterojunction entails the separate fabrication of p-type CdTeNRs and SiNWs array. The p-type CdTeNRs were synthesized by using CdTe power (99.99%) as the source material in a horizontal alumina tube furnace at 650 °C *via* a chemical vapor deposition (CVD) method, during which Sb dopants were incorporated into the CdTeNRs to improve their p-type conductivity.[18] The vertical SiNWs array were prepared in this work by using a Ag-assisted chemical etching approach and n-type Si wafers with a resistivity 4–7 Ω cm^{-1}.[19] After etching, the as-obtained SiNWs array were dipped into a diluted HNO$_3$ and HF solution to dissolve Ag and SiO$_2$ on the surface of SiNWs, respectively. The morphologies and structures of the as-prepared CdTe:Sb NRs and the SiNWs arrays were characterized by scanning electron microscopy (SEM, FEI Quanta 200 FEG), X-ray diffraction (XRD, Rigaku D/Max-rB), X-ray photoelectron spectroscopy (XPS, Thermo ESCALAB 250) and high-resolution transmission electron microscopy (HRTEM, JEOL JEM-2010).

Device fabrication

The device fabrication process starts with the preparation of SiNWs arrays pattern. Firstly, photoresistance windows were defined on the Si wafer by using a UV aligner (BG-401A), and then the patterned SiNWs array were obtained by Ag-assisted chemical etching in the regions where the Si wafer was exposed. Prior to the photolithography, the Si wafer was ultrasonically cleaned in alcohol and acetone in turn. Then, a Si$_3$N$_4$ insulating layer (400 nm) was deposited using a magnetron sputtering system (JGP-560) followed by an additional adjusted photolithography process. Afterwards, the CdTeNRs were mechanically transferred onto the Si substrate with coated Si$_3$N$_4$ film *via* a contact printing technique.[20] By carefully controlling the pressure between the growth substrate and consequently the frictional force between the CdTeNRs and the Si substrate, the density of the CdTeNRs on the SiNWs array could be readily adjusted. The heterojunctions were formed at the regions where the bottom surface of the NRs contacts with the tips of n-SiNWs. Finally, Cu/Au (4 nm/80 nm) double-layer electrodes were deposited on the two ends of the CdTeNR through a high-vacuum electron beam evaporation system (DZS-500), and indium–gallium alloy (In–Ga) was daubed on the back side of the Si substrate as the electrode for the SiNWs array.

Device characterization

The device characteristics of the p-CdTeNR/n-SiNWs array heterojunctions were measured by using a semiconductor characterization system (Keithley 4200-SCS) on a probe station. The photovoltaic performance of the devices was further studied by using a solar simulator (San-Ei Electric, XES-301S,

100 mW cm^{-2}). To determine the spectral response and time response of the heterojunction devices, a home-built system composed of a light source (LE-SP-LS-XE), a monochromator (LE-SP-M300), an oscilloscope (Tektronix, TDS2012B), and an optical chopper (LE-oc120) was used.

Results and discussion

Fig. 1a shows a typical SEM image of the Sb-doped CdTeNRs, from which it can be seen that the NRs are sparsely grown on the underlying large crystals. The width of the NRs ranges from several hundreds of nanometers to a few micrometers, while the length is around several tens of micrometers. The corresponding energy-dispersive X-ray spectroscopy (EDX) profile shown in the inset of Fig. 1a reveals that the atomic ratio of the Cd : Te is about 51 : 49, which is very close to the stoichiometric ratio of CdTe. Fig. 1b depicts the XRD pattern of the CdTe:Sb NRs, from which it is found that all the peaks could be readily assigned to CdTe with zinc blende structure (JCPDS 89-3053). The doped Sb was confirmed by XPS analysis in which two Sb 3d peaks with binding energy of 530 eV and 539.5 eV, and a Sb 3p peak with binding energy of 768.3 eV can be observed, with a doping concentration of 4.65% (atomic ratio). The HRTEM image and the corresponding fast Fourier transform (FFT) pattern recorded on the tip of a single NR reveal that the Sb-doped CdTeNRs have a single crystal zinc blende structure with a growth orientation of [211] (Fig. 1d).

The as-prepared Sb-doped CdTeNRs were then utilized to fabricate the nano-heterojunction. The step-wise process for the device construction is illustrated in Fig. 2. Briefly, it can be divided into four steps. (1) Fabrication of patterned SiNWs. (2) Deposition of Si$_3$N$_4$ thin-film. (3) Transfer of CdTe NRs. (4) Formation of ohmic contact. The SiNWs were fabricated by using a chemical etching method. Fig. 3a and b show the top-down view of the patterned SiNWs array at different magnifications. It is seen that the patterned SiNWs arrays are uniform among a large area with well-defined pattern. Further HRTEM image of an individual SiNWs and corresponding FFT pattern (Fig. S1†) show that the SiNWs have single crystal structure with the axis along the [100] crystallographic direction.

Fig. 4a displays a typical SEM image of the p-CdTeNR and n-SiNWs array heterojunction device. It can be found that the long CdTeNR crosses between the two Cu/Au electrodes and contacts with SiNWs array to form the heterojunction. I–V characteristics of CdTeNR were first tested, showing good ohmic contact formed between CdTeNR and metal electrodes (Fig. S2†). Fig. 4b plots a typical I–V curve of the p-CdTeNR/n-SiNWs array heterojunction in the dark, revealing an excellent rectification behavior with a rectification ratio of 10^5 at ± 2 V. Based on this curve, a turn-on voltage of 1.1 V can be deduced at the forward bias. What is more, according to the semilog I–V plots shown in Fig. 4b, the ideality factor n is determined to be 1.79. This value is superior to that of ZnTe:Sb/Si p–n heterojunctions.[21]

Notably, as shown in Fig. 4(c), under AM 1.5 G illumination, the heterojunction device exhibited excellent photovoltaic behavior with an open circuit voltage (V_{OC}) of 0.275 V and short circuit current density (J_{SC}) of 15.08 mA cm^{-2}. The fill
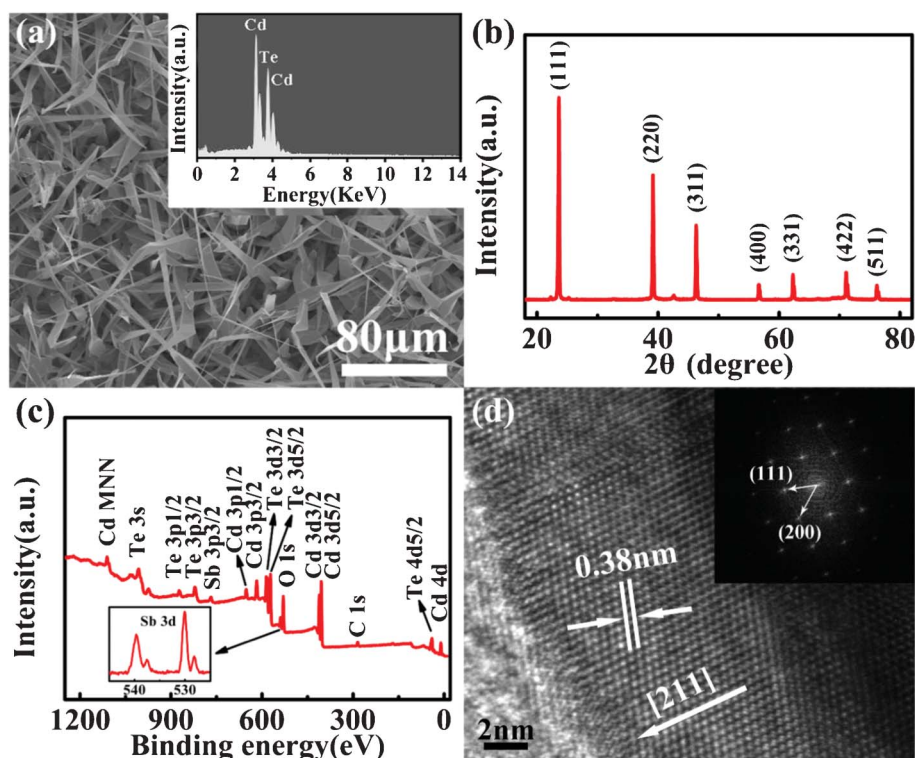
Fig. 1 (a) Typical SEM images of as-prepared CdTe:Sb NRs. Inset shows the corresponding EDX spectrum. (b) XRD pattern of the CdTe:Sb NRs. (c) XPS spectrum of the CdTe:Sb NRs. Inset shows the enlarged Sb $3d_{5/2}$ and Sb $3d_{3/2}$ peaks. (d) HRTEM image of the CdTe:Sb NR. Inset shows the corresponding FFT pattern.

factor (*FF*) and power conversion efficiency (η) of the devices could be deduced from the following equations:

$$FF = I_m V_m / I_{sc} V_{oc} = J_m V_m / J_{sc} V_{oc} \qquad (1)$$

$$\eta = I_m V_m / S P_{in} \qquad (2)$$

where I_m (J_m) and V_m are the current (current density) and voltage at the maximum power output, respectively, S is the active light collection area, which in our case, is the area of CdTeNR on the tips of SiNWs in channel, and P_{in} is the incident light intensity (100 mW cm^{-2}). On the basis of the above equations, *FF* and η are estimated to be 0.49 and 2.1%, respectively. For comparison purpose, heterojunction composed of p-CdTeNR and planar n-Si was also considered. Fig. 4c compared photovoltaic characteristics of the both devices with and without AM 1.5 G illumination. Clearly, one can see that the planar Si-based device showed similar photovoltaic characteristics with the SiNWs array device. The V_{OC} for planar Si device was 0.315 V, which is slightly higher than that of the SiNWs array device while the J_{SC} for planar Si device was only 8.57 mA cm^{-2}, smaller than that of the SiNWs array device. The decrease in V_{OC} for the SiNWs array device is assumed to be associated with the huge surface-to-volume ratio of SiNWs, which is in good agreement with previous work on macroporous silicon photoelectrochemical cells.[22] As established in our previous work, unlike planar Si, SiNWs fabricated from n-type silicon wafer *via* a metal-assisted chemical etching method tend to exhibit reduced n-type or even p-type conduction behavior due to surface absorption, termination, or passivation.[13,23,24]
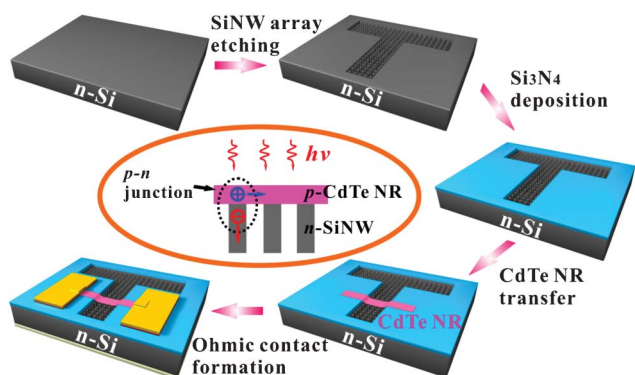
Fig. 2 Schematic illustration of the fabrication process for the p-CdTeNR/n-SiNW array heterojunction device.
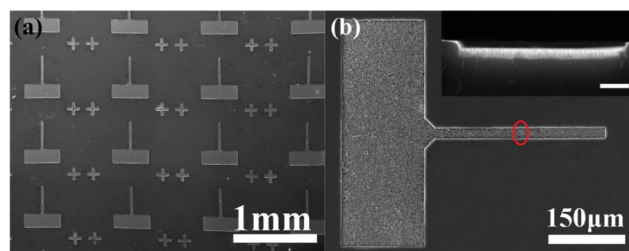
Fig. 3 (a) and (b) are typical SEM images of patterned SiNW arrays. Inset in (b) shows the cross-sectional SEM image of a patterned SiNW array, the scale bar is 5 μm.
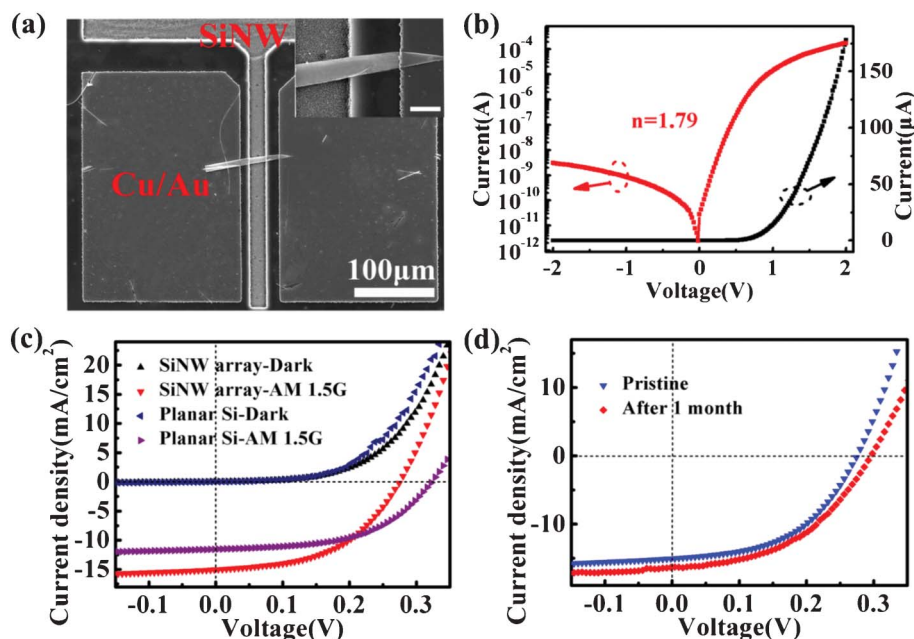
Fig. 4 (a) SEM images of a typical p-CdTeNR/n-SiNW array heterojunction device. The inset shows a magnified SEM image of the device, the scale bar is 10 μm. (b) Rectification characteristics of the CdTeNR/SiNW array heterojunction measured in the dark. (c) Photovoltaic characteristics of the CdTeNR/SiNW array heterojunction device and CdTeNR/planar Si heterojunction device measured in dark and AM 1.5 G illumination (100 mWcm^{-2}). (d) Photovoltaic characteristics of the CdTeNR/SiNW array heterojunction device over time.

This transform in electrical property leads to weakened built-in field between the p-CdTeNR and n-Si which is responsible for the reduced V_{OC} in SiNWs array device. It should be mentioned that although the effective contact area of CdTeNR/SiNWs array junction (tips of SiNWs) is virtually negligible, compared with the planar Si-based solar cell, it does not necessarily mean low energy conversion efficiency. We attributed the observed higher efficiency of SiNWs array based solar cell to the improved light absorption, trapping effect, and effective carrier transport.[12,13] The FF and η for planar Si device are calculated to be 0.52 and 1.4% according to the eqn (1) and (2), respectively. Note that S in eqn (2) was regarded as the area of CdTeNR on the surface of planar Si in the channel.

Next, to explore the possibility of our devices for long-term solar light harvesting, we studied the photovoltaic characteristic of the CdTeNR/SiNWs array device as a function of storage time. As shown in Fig. 4d, after 1 month storage in air, the device exhibited a slight promotion in photovoltaic performance. The V_{OC} and the J_{SC} are 0.296 V and 16.34 mA cm^{-2}, respectively; what is more, the corresponding FF and η are respectively calculated to be 0.47 and 2.3%. The observed increase in V_{OC} and J_{SC} can be ascribed to the presence of the native oxide layer at the surface of SiNWs. It is well known that a thin layer of silicon oxide (SiO or SiO$_2$) can form on SiNWs surface when exposed in ambient conditions.[25] Such oxide layer will allow more efficient transport of minority carriers and collection by electrode in that they will serve as efficient passivation layer where the velocity recombination of minority carriers is largely restricted.[25] On the other hand, the native oxide layer formed on the Si surface can strengthen the built-in field between CdTeNR and SiNWs array by preventing SiNWs from absorbing water and gas molecules. Therefore, it is also beneficial to device performance.

The working mechanism of the heterojunction photovoltaic device can be qualitatively elucidated by the energy band diagram of p-CdTeNR/n-SiNWs array heterojunction shown in Fig. 5a. As mentioned above, a built-in field is formed at the CdTe and SiNWs interface with the direction from SiNWs to CdTe, as a result of their differences in work functions. Upon incident light illumination, a massive amount of electron-hole pairs on both the CdTeNR and the SiNWs sides will be generated. When the electron-hole pairs diffuse to the interface of CdTeNR and the SiNWs, they will be separated by the built-in field and collected by the electrodes. These carriers continue to move and finally form the photocurrent in circuit. Remarkably, the unique structure of the heterojunction devices is significant to energy conversion. Due to the difference in band gap (CdTe 1.5 eV vs. Si 1.12 eV), the CdTeNR mainly absorbs light in visible to the ultraviolet region, whilst the SiNWs array prefer to absorb light with longer wavelength, namely from the visible to the near-infrared region. Therefore, the distinct device structure of the CdTeNR/SiNWs array heterojunction ensures that incident light over a wide spectrum can be efficiently absorbed and utilized as well as promoting a light-trapping effect. This feature is superior to those of the conventional crystal Si-based solar cells, which show poorer absorption in the short wavelength range.

In addition to photovoltaic application, the p-CdTeNR/n-SiNWs array heterojunction devices could act as high-performance photodetectors for visible to NIR light illumination as well. Fig. 5a depicts the spectral response of the heterojunction device to light illumination ranging from ultraviolet to NIR. Clearly, one can see that the highest sensitivity is located at around 930 nm. This spectral selectivity is understandably associated with the working mechanism of the device. As shown in Fig. 5b, under light illumination, partial photons with energy
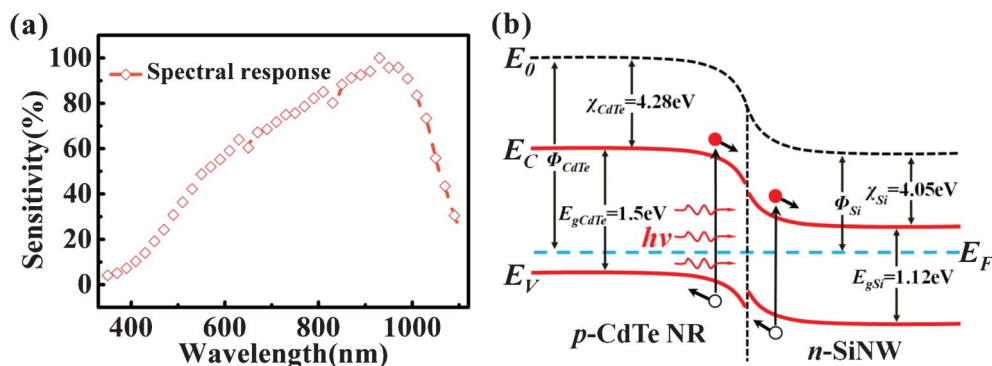
Fig. 5 (a) Spectral response of CdTeNR/SiNW array heterojunction device. During the spectral response study, the light intensity was kept at the same value. (b) Energy band diagram of CdTeNR/SiNW array heterojunction upon light illumination.

larger than the band gap of CdTe (E_{gCdTe}) and all photons with energy smaller than E_{gCdTe} could penetrate the thin CdTeNR and arrive at the heterojunction area. Amongst these photons, only those with energy larger than the band gap of crystal Si (E_{gSi}) could be absorbed by SiNWs and finally contribute to the photocurrent. Fig. 6a shows the dependence of the heterojunction devices photocurrent under light illumination of various intensities. It can be found that the photocurrent increases almost linearly with the increase of light intensity, signifying the high quality of the heterojunction. To further study the stability and reproducibility of the heterojunction photodetectors, the photoresponse characteristics of the device under light illumination of different intensities were investigated. As observed from Fig. 6b, the electrical current increases sharply and is stabilized at a high-conduction 'on' state after upon light radiation, but it decreased quickly to a low-conductivity 'off' state after light illumination was turned off, leading to an on/off ratio as high as 10^4. Compared with previous photodetectors solely made of CdTe nanostructures,[8,9] our p-CdTeNR/n-SiNWs array heterojunction photodetectors shows improved photocurrent on/off ratio. This improvement in performance is expressly due to the unique device configuration.

To explore the potential application for light-wave communication and in optical switches, the photoresponse of the p-CdTeNR/n-SiNWs array heterojunction devices was further

studied by using an oscilloscope to monitor the variation of the photocurrent under pulsed light, which was generated by a mechanical chopper (Fig. 7a). It was interesting to find that our device could work over a wide frequency range from 50 to 600 Hz under white light illumination with an intensity of 62.5 μW cm^{-2}, with excellent stability and reproducibility (Fig. 7b–d). Notably, even at 600 Hz, the $[I_{max} - I_{min}/I_{max}]$ value only decreases by less than 20% (Fig. 7e), this means that our device is capable of monitoring pulsed light with very high frequency. In the time domain, the speed of a photodetector is often evaluated by the rise time (τ_r) and the fall time (τ_f) of its response to an impulse signal or to a pulse signal. The τ_r is the time interval for the response to rise from 10 to 90% of its peak value, and the τ_f is the time interval for the response to decay from 90 to 10% of its peak value.[26,27] Careful analysis of the p-CdTeNR/n-SiNWs array heterojunction device reveals a small τ_r of 1.2 ms and a small τ_f of 1.58 ms (Fig. 7f), respectively. These values are much faster than the reported CdTe NWs and CdTeNRs based photodetectors.[7–9] Such fast response speed could be associated with the high-quality heterojunction formed between the CdTeNR and the SiNWs array, which facilitates the effective and rapid separation of the photo-generated carriers. Considering the fact that the response speed is highly dependent on light intensity, both τ_r and τ_f could be further reduced by increasing the light intensity.[28]
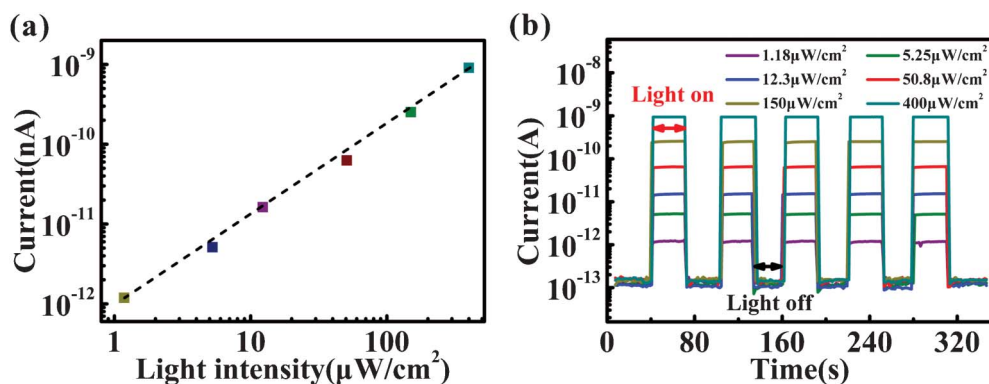
Fig. 6 (a) The dependence of photocurrent on light intensity at zero bias. (b) Photoresponse of the CdTeNR/SiNW array heterojunction device under various light intensities.
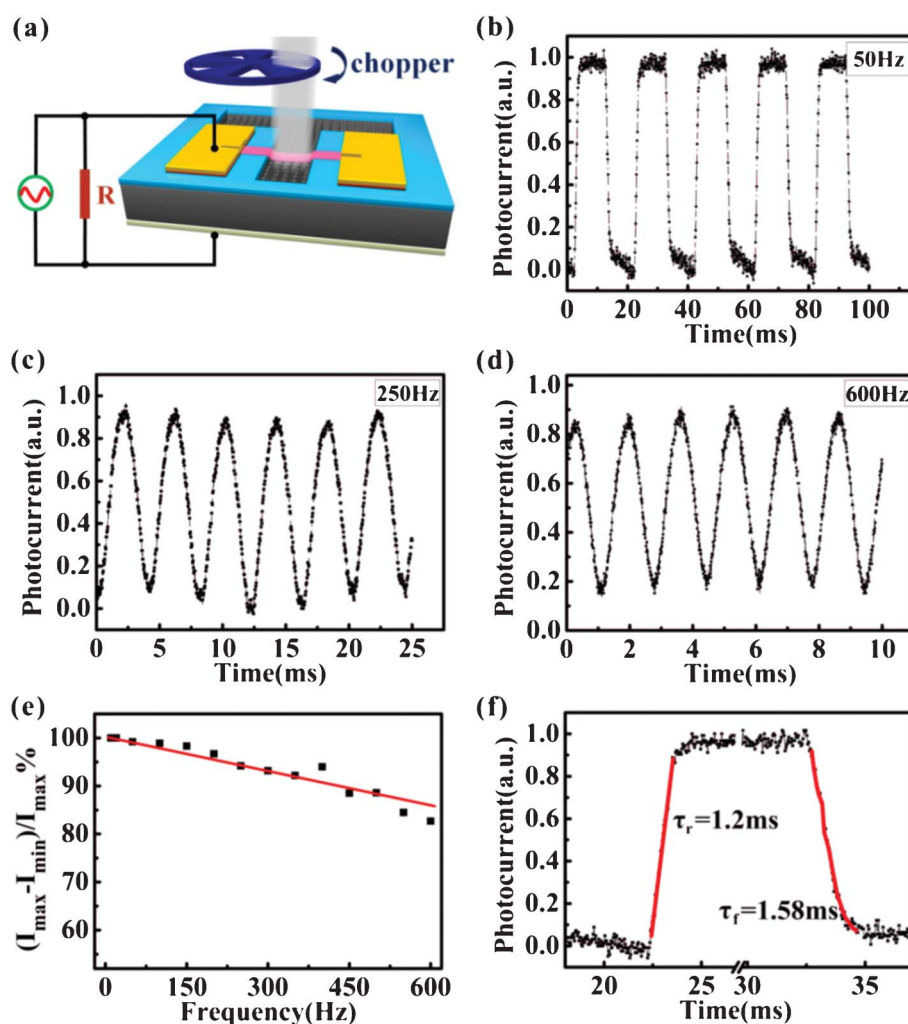
Fig. 7 (a) Schematic illustration of the measurement configuration for photoresponse detection. Photoresponse characteristics of the CdTeNR/SiNW array heterojunction device to pulsed light irradiation at frequencies of (b) 50 Hz, (c) 250 Hz and (d) 600 Hz. (e) The relative balance $[(I_{max} - I_{min})/I_{max}]$ *versus* switching frequency. (f) Rising and falling edges for estimating τ_r and τ_f.

Conclusion

In conclusion, high quality p-CdTeNR/n-SiNWs array hetero-junctions for photovoltaic device and photodetector applications were constructed by a convenient route. The heterojunction exhibited pronounced rectification characteristics with rectification ratio of approximately 10^5 at ± 2 V in the dark. Due to the matched band gaps and the novel heterojunction architecture, prominent photovoltaic behavior with energy conversion efficiency up to 2.1% under AM 1.5 G illumination and long-term stability were observed. Furthermore, the devices demonstrated high sensitivity to the visible-NIR illumination under zero bias with high photosensitivity ($\sim 6.3 \times 10^3$), fast response speed ($\tau_r = 1.2$ ms, $\tau_f = 1.58$ ms) and excellent stability and reproducibility in a wide range of switching frequencies (50–600 Hz). It is expected that this new p-CdTeNR/n-SiNWs array heterojunction structure will have promising potential for future applications in nano-semiconductor heterojunction optoelectronic devices.

Acknowledgements

References

1 J. Britt and C. Ferekides, *Appl. Phys. Lett.*, 1993, **62**, 2851.
2 Y. Tomita, T. Kawai and Y. Hatanaka, *Jpn. J. Appl. Phys.*, 1994, **33**, 3383.
3 J. S. Jie, W. J. Zhang, I. Bello, C. S. Lee and S. T. Lee, *Nano Today*, 2010, **5**, 313.
4 J. Britt and C. Ferekides, *Appl. Phys. Lett.*, 1993, **62**, 2851.
5 X. Z. Wu, *Sol. Energy*, 2004, **77**, 803.
6 X. N. H. Wang, J. Zhu, Y. M. Xu, H. Wang, Y. Tao, S. K. Hark, X. D. Xiao and Q. Li, *ACS Nano*, 2010, **4**, 3302.
7 M. C. Kum, H. Jung, N. Chartuprayoon, W. Chen, A. Mulchandani and N. V. Myung, *J. Phys. Chem. C*, 2012, **116**, 9202.
8 Y. Ye, L. Dai, T. Sun, L. P. You, R. Zhu, J. Y. Gao, R. M. Peng, D. P. Yu and G. G. Qin, *J. Appl. Phys.*, 2010, **108**, 044301.
9 X. Xie, S. Y. Kwok, Z. Z. Lu, Y. K. Liu, Y. L. Cao, L. B. Luo, J. A. Zapien, I. Bello, C. S. Lee, S. T. Lee and W. J. Zhang, *Nanoscale*, 2012, **4**, 2914.
10 A. I. Hochbaum, R. Fan, R. R. He and P. D. Yang, *Nano Lett.*, 2005, **5**, 457.

11 M. L. Zhang, K. Q. Peng, X. Fan, J. S. Jie, R. Q. Zhang, S. T. Lee and N. B. Wong, *J. Phys. Chem. C*, 2008, **112**, 4444.

12 E. Garnett and P. D. Yang, *Nano Lett.*, 2010, **10**, 1082.

13 J. S. Jie, W. J. Zhang, K. Q. Peng, G. D. Yuan, C. S. Lee and S. T. Lee, *Adv. Funct. Mater.*, 2008, **18**, 3251.

14 E. C. Garnett and P. D. Yang, *J. Am. Chem. Soc.*, 2008, **130**, 9224.

15 V. Sivakov, G. Andrä, A. Gawlik, A. Berger, J. Plentz, F. Falk and S. H. Christiansen, *Nano Lett.*, 2009, **9**, 1549.

16 D. Wu, Y. Jiang, S. Y. Li, F. Z. Li, J. W. Li, X. Z. Lan, Y. G. Zhang, C. Y. Wu, L. B. Luo and J. S. Jie, *Nanotechnology*, 2011, **22**, 405201.

17 X. J. Shen, B. Q. Sun, D. Liu and S. T. Lee, *J. Am. Chem. Soc.*, 2011, **133**, 19408.

18 L. Zhu, J. S. Jie, D. Wu, L. B. Luo, C. Y. Wu, Z. F. Zhu, Y. Q. Yu and L. Wang, *J. Nanoeng. Nanomanuf.*, 2012, **2**, 1.

19 L. B. Luo, J. S. Jie, W. F. Zhang, Z. B. He, Z. H. Chen, J. X. Wang, W. J. Zhang, C. M. Wu and S. T. Lee, *Appl. Phys. Lett.*, 2009, **94**, 193101.

20 Z. Y. Fan, J. C. Ho, T. Takahashi, R. Yerushalmi, K. Takei, A. C. Ford, Y. L. Chueh and A. Javey, *Adv. Mater.*, 2009, **21**, 3730.

21 D. Wu, Y. Jiang, Y. G. Zhang, J. W. Li, Y. Q. Yu, Y. P. Zhang, Z. F. Zhu, L. Wang, C. Y. Wu, L. B. Luo and J. S. Jie, *J. Mater. Chem.*, 2012, **22**, 6206.

22 J. R. Maiolo III, H. A. Atwater and N. S. Lewis, *J. Phys. Chem. C*, 2008, **112**, 6194.

23 C. S. Guo, L. B. Luo, G. D. Yuan, X. B. Yang, R. Q. Zhang, W. J. Zhang and S. T. Lee, *Angew. Chem., Int. Ed.*, 2009, **48**, 9896.

24 L. B. Luo, X. B. Yang, F. X. Liang, H. Xu, Y. Zhao, X. Xie, W. F. Zhang and S. T. Lee, *J. Phys. Chem. C*, 2011, **115**, 18453.

25 F. T. Zhang, B. Q. Sun, T. Song, X. L. Zhu and S. T. Lee, *Chem. Mater.*, 2011, **23**, 2084.

26 L. B. Luo, F. X. Liang and J. S. Jie, *Nanotechnology*, 2011, **22**, 485701.

27 L. B. Luo, J. S. Jie, Z. H. Chen, X. J. Zhang, X. Fan, G. D. Yuan, Z. B. He, W. F. Zhang, W. J. Zhang and S. T. Lee, *J. Nanosci. Nanotechnol.*, 2009, **9**, 6292.

28 Y. Jiang, W. J. Zhang, J. S. Jie, X. M. Meng, X. Fan and S. T. Lee, *Adv. Funct. Mater.*, 2007, **17**, 1795.